

A Hh-driven gene network controls specification, pattern and size of the *Drosophila* simple eyes

Daniel Aguilar-Hidalgo^{1,2,*}, María A. Domínguez-Cejudo^{1,*}, Gabriele Amore³, Anette Brockmann^{1,†},
María C. Lemos², Antonio Córdoba² and Fernando Casares^{1,§}

SUMMARY

During development, extracellular signaling molecules interact with intracellular gene networks to control the specification, pattern and size of organs. One such signaling molecule is Hedgehog (Hh). Hh is known to act as a morphogen, instructing different fates depending on the distance to its source. However, how Hh, when signaling across a cell field, impacts organ-specific transcriptional networks is still poorly understood. Here, we investigate this issue during the development of the *Drosophila* ocellar complex. The development of this sensory structure, which is composed of three simple eyes (or ocelli) located at the vertices of a triangular patch of cuticle on the dorsal head, depends on Hh signaling and on the definition of three domains: two areas of *eya* and so expression – the prospective anterior and posterior ocelli – and the intervening interocellar domain. Our results highlight the role of the homeodomain transcription factor *engrailed* (*en*) both as a target and as a transcriptional repressor of *hh* signaling in the prospective interocellar region. Furthermore, we identify a requirement for the *Notch* pathway in the establishment of *en* maintenance in a Hh-independent manner. Therefore, *hh* signals transiently during the specification of the interocellar domain, with *en* being required here for *hh* signaling attenuation. Computational analysis further suggests that this network design confers robustness to signaling noise and constrains phenotypic variation. In summary, using genetics and modeling we have expanded the ocellar gene network to explain how the interaction between the Hh gradient and this gene network results in the generation of stable mutually exclusive gene expression domains. In addition, we discuss some general implications our model may have in some Hh-driven gene networks.

KEY WORDS: Ocellus, *hedgehog*, Patterning, Mathematical model, Retinal determination genes, Gene network, *Drosophila*, *engrailed*, *Notch*

INTRODUCTION

During development, gradients of intercellular signals (called morphogens) are read and modified dynamically by fields of target cells. As a result, spatiotemporal patterns of gene expression are generated. These patterns are then translated into cell function and into the development of functional body structures (Freeman and Gurdon, 2002; Davidson, 2006). Yet how the integration between intercellular signals and intracellular gene networks occurs is only beginning to be understood.

One of the best characterized family of morphogens is that of *hedgehog* (*hh*). Hh genes are evolutionarily conserved and participate in many key developmental processes. Not surprisingly, their malfunction has been associated with a number of developmental diseases and with cancer (Jiang and Hui, 2008; Varjosalo and Taipale, 2008; Ingham et al., 2011). Experimental work in *Drosophila* and in vertebrates indicates that the Hh signaling pathway is subject to extensive feedback among elements of the pathway, most notably that of the Hh receptor *patched* (*ptc*) (Chen and Struhl, 1996; Marigo and Tabin, 1996). Furthermore, the combination of experimental and modeling studies on developing fly wings and on vertebrate neural tube and limbs have uncovered new roles for this feedback in the dynamics of Hh gradient formation, in

its robustness and in the generation of distinct patterns of target gene expression (Briscoe et al., 2001; Saha and Schaffer, 2006; Dessaud et al., 2007; Dessaud et al., 2008; González et al., 2008; Nahmad and Stathopoulos, 2009; Dessaud et al., 2010; Irons et al., 2010; Probst et al., 2011; Balaskas et al., 2012). Therefore, the iteration between mathematical modeling and experimentation is emerging as a productive way of illuminating the problem of Hh morphogen action during organ growth and patterning. Here, we investigate this issue in a particularly simple and genetically tractable model organ: the *Drosophila* ocellar complex.

The *Drosophila* ocelli are three simple eyes [one anterior (or medial) ocellus and two posterior (or lateral) ocelli] located at the vertices of a triangular patch of cuticle on the dorsal head. Together, the ocelli and the interocellar cuticle (plus its bristles) are referred to as the ‘ocellar complex’ (Fig. 1A). The development of the ocellar complex depends on *hh*. Flies homozygous for a *hh* temperature-sensitive mutation raised at the restricted temperature during larval development (Royet and Finkelstein, 1996) or expressing a dominant-negative Ptc receptor [PtcΔloop2 (Briscoe et al., 2001)] lack the ocellar complex (Fig. 1B). Therefore, *hh* signaling is required for the specification and pattern of two tissue types: ocellus and interocellar cuticle.

The ocellar complex forms by the fusion of the dorsal-anterior domains of the eye discs (Haynie and Bryant, 1986). Here, the ocellar field is specified by the action of, at least, two transcription factors: the *pax6* gene *twin of eyeless* (*toy*) and the Otx family member *orthodenticle* (*otd*) (*ocelliless*, *oc* – FlyBase) (Finkelstein et al., 1990; Wieschaus et al., 1992; Royet and Finkelstein, 1995; Punzo et al., 2002; Blanco et al., 2010; Wang et al., 2010; Brockmann et al., 2011). *hh* is expressed within the ocellar field in the prospective interocellar region (Royet and Finkelstein, 1996;

¹CABD (CSIC-UPO-Junta de Andalucía), Sevilla 41013, Spain. ²Condensed Matter Physics Department Universidad de Sevilla, Sevilla 41012, Spain. ³Istituto Regionale Vini e Oli di Sicilia, Palermo 90143, Italy.

*These authors contributed equally to this work

†Present address: University of Konstanz, Konstanz 78457, Germany

§Author for correspondence (fcasfer@upo.es)

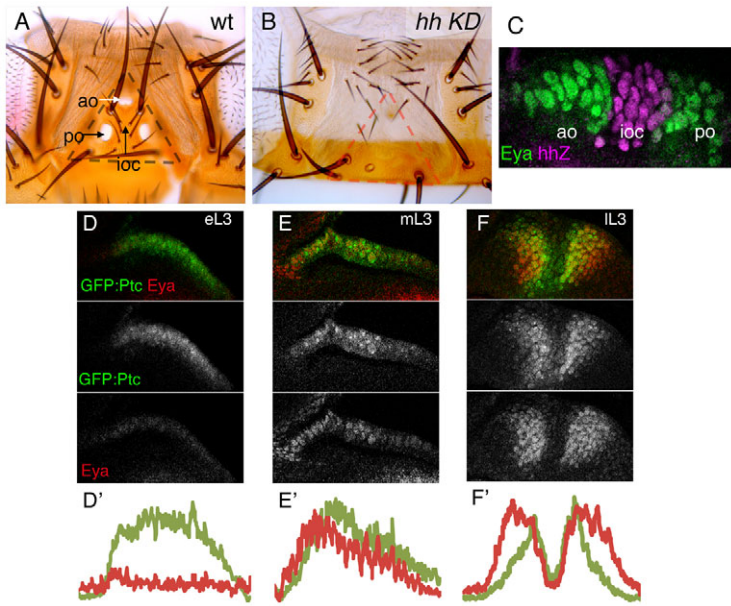


Fig. 1. Dynamic *hh* signaling and the development of the ocellar complex. (A, B) Dorsal views of adult heads from wild-type (A) or *oc2>ptcΔloop2* (*hh* signaling knock down; *hhKD*). The ocellar complex is outlined by the triangle. Anterior ocellus (ao), posterior ocellus (po) and interocellar cuticle (ioc) are marked. All elements of the ocellar complex are obliterated when the *hh* signaling pathway is blocked. (C) Ocellar region of a late L3 disc from a *hhZ* larvae. The β-galactosidase-expressing domain (magenta; *hhZ*) labels the prospective interocellar cuticle (ioc) and is flanked by two domains of *Eya* expression (green) in the prospective anterior (ao) and posterior (po) ocelli. This orientation (anterior towards the left) will be maintained throughout. (D-F') Prospective ocellar regions of early ('e', D), mid ('m', E) and late ('l', F) third instar (L3) GFP:Ptc larvae, stained for anti-*Eya*. GFP signal was detected directly. Merged and single channels are shown. Below, signal intensity histograms of both GFP:Ptc (green) and *Eya* (red) signals of the respective discs. GFP:Ptc, which is used as a read-out of the Hh signaling, is initially expressed at high uniform levels through the region (D-E'), to later evolve into a high-low-high pattern (E', F'). *Eya* expression is detected at low and uniform levels in eL3 (D, D'), to then increase as a single domain in mL3 (E, E'), which is later transformed into a high-low-high pattern similar to Ptc (F, F').

Royet and Finkelstein, 1997). The retinal determination (RD) genes *eyes absent* (*eya*) and *sine oculis* (*so*) are required for the formation of the ocelli (Bonini et al., 1993; Cheyette et al., 1994; Serikaku and O'Tousa, 1994; Bonini et al., 1998; Blanco et al., 2009; Blanco et al., 2010; Brockmann et al., 2011). Both *eya* and *so* are expressed with identical patterns in two domains flanking *hh*, and mark the prospective ocelli in late third larval (L3) stage discs (Blanco et al., 2009). The expression of *eya* and *so* depends on secreted Hh and on their mutual positive feedback (Pauli et al., 2005; Blanco et al., 2009). In addition to the activation of *eya* and *so*, expression of the TALE-homeodomain transcription factor *homothorax* (*hth*) is concomitantly repressed in the ocellar domains. Otherwise, maintenance of *hth* expression prevents ocellar development (Brockmann et al., 2011).

In this paper, we have investigated how the single domain of *hh* expression is capable of generating the ocellar pattern through the regulation of a downstream gene network using both genetic and modeling approaches.

MATERIALS AND METHODS

Drosophila strains and genetic manipulations

oc2-GAL4 (Blanco et al., 2009) was used to drive UAS lines specifically in the developing dorsal anterior region of the eye-antennal imaginal disc (EAD), where the ocellar region derives from. In the case of UASdsRNAi strains, crosses were raised at 29°C, to maximize the penetrance of the knock-downs. Other crosses were set at 25°C. UAS lines used were as follows: UAS-GFP-*ptcΔloop2* [UAS-*ptcDN* (Briscoe et al., 2001)], UAS-*ci* (Alexandre et al., 1996), UAS-*mamDN* (dominant negative) (Kumar and Moses, 2001) and UAS-*en* (Guillén et al., 1995; Tabata et al., 1995); the *hedgehog* transcriptional reporter line *hh^{P30}* (referred to herein as *hh-Z*) and the *engrailed* transcriptional reporter line *en^{Xho25}* (referred to herein as *en-Z*), which are from the Bloomington Stock Center (<http://flystocks.bio.indiana.edu>); and UAS-*DIRNAi* (28032) and UAS-*Su(H)RNAi* (103597), which are from the VDRC (<http://stockcenter.vdrc.at/control/main>). The GFP:Ptc strain [CB02030 from Flytrap (<http://flytrap.med.yale.edu/>) (Buszczak et al., 2007)] is a GFP-protein trap that tags the Ptc product. Two reference strains, Oregon-R (Or-R) and *w¹¹¹⁸*, and stocks carrying mutant alleles for *patched* [*ptc*: *yw*; *FRT42 ptc^{S2}/CyO* (BL # 6332)], *smoothed* (*smo*: *w*; *smo³ FRT40A/CyO*), *cubitus interruptus* (*ci*: *ywhsflp*; *Ci+ FDT40A/CyO*; ; *Ci⁹⁴*) and *Notch* [*N*: *w[ch2]*, *N²⁶⁴⁻³⁹/FM4*, *B[+]* (BL # 730)] are described in FlyBase.

The flip-out method (Basler and Struhl, 1994) was used to induce gain-of-function clones. Clones were induced 48-72 hours after egg laying (AEL) by a 10 heat-shock at 35.5°C in larvae from the cross of *yw*, *hs-flp*, *act>hsCD2>Gal4*; *UAS-lacZ* females with UAS-*hthGFP* males (*hth+* clones) or *yw*, *hs-flp*, *act>hsCD2>Gal4*; *UAS-GFP* females with UAS-*en* males (*en+* clones). *en* loss-of-function clones were generated through mitotic recombination (Xu and Rubin, 1993) in *yw*, *hs-flp*; *FRT42D Df(2R)en^F/FRT42D*, *ubiGFP* larvae. *Df(2R)en^F* deletes both the *engrailed* and *invected* paralogous genes (described in FlyBase). Clones were induced 48-72 hours AEL by a 45 heat-shock at 37°C. Clones were marked in larval tissues by the absence of GFP. Adult heads from this experiment were mounted and their dorsal head examined for ocellar field defects. Clones were not marked in the adult.

Adult cuticle preparation and quantifications

Dorsal head cuticle pieces were dissected from adult or late pharate heads in PBS, and mounted in Hoyers solution:acetic acid (1:1), as described previously (Casares and Mann, 2000). Images were obtained in a Leica DM500B microscope with a Leica DFC490 digital camera and processed with Adobe Photoshop. Ocellar (longest axis) and interocellar lengths were measured with ImageJ (<http://imagej.nih.gov/ij/>) on digital images and expressed in pixels.

Immunostaining and imaging

Immunofluorescence was carried out as described previously (Bessa and Casares, 2005). Antibodies used were: guinea pig anti-Hth (Casares and Mann, 2000), guinea pig anti-So (Mutsuddi et al., 2005), rabbit anti β-galactosidase (Cappel), mouse anti-Ptc (Nakano et al., 1989), mouse anti-*Eya* (10H6), mouse anti-*En* (4D9), mouse anti-*Dl* (C594.9B) and rat anti-*CiA* (2A1) [which detects the activator form of *Ci* (Aza-Blanc et al., 1997; Méthot and Basler, 1999); all from the Developmental Studies Hybridoma Bank, University of Iowa (<http://dshb.biology.uiowa.edu>)]. Appropriate Alexa-conjugated secondary antibodies were used. Nuclei were counterstained with DAPI. Image acquisition was carried out in an Apotome Zeiss Axio Imager M2 fluorescence microscope and a Leica SME confocal system. Images were processed with Adobe Photoshop.

Expression profiles

Confocal sections of GFP:ptc eye discs at different stages of L3 development, and co-stained with anti-*Eya*, were selected. To ensure that only signal coming from the prospective ocellar regions were analyzed, each of these regions was outlined with the lasso tool, copied and pasted on a black background and saved as a TIFF file, using Adobe Photoshop. The expression profiles were obtained from these TIFF files using ImageJ.

Temperature fluctuation assay

A temperature fluctuation assay was carried out essentially as previously (Li et al., 2009). Embryos were collected for 24 hours (at 25°C) and grown for an additional 24 hours at 25°C and then transferred to 31°C until larvae reached third instar. Then, larvae were subjected to five cycles of temperature pulses (1.5 hours at 18°C + 1.5 hours at 31°C). After these pulses, cultures were maintained at 25°C until eclosion. As controls, the same strains were grown at constant 25°C throughout development.

Model implementation

A simplified one-cell model (13 equations) was implemented using Vensim software, a visual tool for solving ODEs that allows parameter values modification in run-time (Vensim PLE version 5.11, Ventana Systems, <http://www.vensim.com/software.html>). This program contains a fourth order Runge Kutta method (RK4) to solve ODE systems. The 31-cell full model was implemented using MATLAB and solved with the integrator ode45.

Complete list of model equations and general descriptions

Each of the 13 differential equations of the reaction-diffusion type describes the behavior of one system variable (gene transcription and protein production) in a row of 31 cells with a symmetrical distribution of cells centered on the morphogen source (five middle cells). Equation 1 describes the classical evolution of a morphogen (Hh) gradient with production and diffusion terms. In this model, the level of complexity was increased by adding a negative regulation, as formation of Ptc/Hh complexes reduces dynamically the concentration of free Hh. The production term is limited to the *hh*-expressing cells, as expressed in Eqn 14.

Following von Dassow et al. (von Dassow et al., 2000), all other equations distinguish between mRNA transcription and translation. Translation is described using linear terms of production and degradation. Transcriptional regulation is described using non-linear terms, either positive or negative, in the form of compound Hill equations. The specific form of these type of terms is $\phi(X\psi(Y, k_2, n_2), k_1, n_1)$, where $\phi(X, k, n) = X^n / (k^n + X^n)$ and $\psi(Y, k, n) = 1 - Y^n / (k^n + Y^n)$. The ocular model contains autoregulations. In these cases, the equation term is described as a simple sigmoid in the form $\phi(X, k, n)$ (see supplementary material Appendix S1 for further details). For each species, the equation takes specific forms, depending on its specific regulatory relationships (for example, with or without autoregulation term).

The model contains different parameter types: α_x for the basal transcription rates, β_x for the degradation rates, k_x for the Hill equation transcriptional regulators, n_x for the Hill coefficients, θ_x for the translation rates and γ_x for protein complex formation. The non-dimensional parameters k_0 , k_{Ci} , k_{En} and k_{Ciptc} are used for changing the scale of different terms and D is the diffusion coefficient. Subscript X-Y, with X and Y system variables, indicates regulation from X to Y. For example, k_{En-ptc} is the Hill transcriptional regulation parameter of the interaction from En to *ptc*. All the reaction-diffusion equations contain a degradation term.

$$\frac{\partial Hh}{\partial t} = D \frac{\partial^2 Hh}{\partial x^2} + \delta(x) \alpha_{hh} - \gamma_{Ptc-Hh} Ptc \cdot Hh - \beta_{Hh} Hh \quad (1)$$

$$\frac{\partial ptc}{\partial t} = \kappa_0 \beta_{ptc} \left\{ \frac{\alpha_{ptc} + \kappa_{Ciptc} \left[\frac{C_A^{nC_{iA}} \left(1 - \frac{C_R^{nC_{iR}}}{k_{C_{iR}}^{nC_{iR}} + C_{iR}^{nC_{iR}}} \right)^{nC_{iA}}}{k_{C_{iA}}^{nC_{iA}} + C_{iA}^{nC_{iA}} \left(1 - \frac{C_R^{nC_{iR}}}{k_{C_{iR}}^{nC_{iR}} + C_{iR}^{nC_{iR}}} \right)^{nC_{iA}} \right]}{\left(1 - \frac{En^{n_{En-ptc}}}{k_{En-ptc}^{n_{En-ptc}} + En^{n_{En-ptc}}} \right) - ptc} \right\} \quad (2)$$

$$\frac{\partial Ptc}{\partial t} = \theta_{ptc} ptc - \gamma_{Ptc-Hh} Ptc \cdot Hh - \beta_{Ptc} Ptc \quad (3)$$

$$\frac{\partial PtcHh}{\partial t} = \gamma_{Ptc-Hh} Ptc \cdot Hh - \beta_{PtcHh} PtcHh \quad (4)$$

$$\frac{\partial ci}{\partial t} = \kappa_0 \beta_{ci} \left\{ \frac{\alpha_{ci} \left(1 - \frac{En^{n_{En-ci}}}{k_{En-ci}^{n_{En-ci}} + En^{n_{En-ci}}} \right)^{nC_i}}{k_{ci}^{nC_i} + \left(1 - \frac{En^{n_{En-ci}}}{k_{En-ci}^{n_{En-ci}} + En^{n_{En-ci}}} \right)^{nC_i}} - ci \right\} \quad (5)$$

$$\frac{\partial C_{iA}}{\partial t} = \kappa_0 \beta_{C_{iA}} \left(\theta_{ci} ci - C_{iA} \right) - \kappa_{Ci} \frac{C_A^{nC_{iA}} \left(1 - \frac{\left(\frac{PtcHh}{Ptc} \right)^{n_{PH}}}{k_{PH}^{n_{PH}} + \left(\frac{PtcHh}{Ptc} \right)^{n_{PH}}} \right)^{nC_{iA}}}{k_{C_{iA}}^{nC_{iA}} + C_{iA}^{nC_{iA}}} \quad (6)$$

$$\frac{\partial C_{iR}}{\partial t} = \kappa_{Ci} \frac{C_A^{nC_{iA}} \left(1 - \frac{\left(\frac{PtcHh}{Ptc} \right)^{n_{PH}}}{k_{PH}^{n_{PH}} + \left(\frac{PtcHh}{Ptc} \right)^{n_{PH}}} \right)^{nC_{iA}}}{k_{C_{iA}}^{nC_{iA}} + C_{iA}^{nC_{iA}}} - \kappa_0 \beta_{C_{iR}} C_{iR} \quad (7)$$

$$\frac{\partial en}{\partial t} = \kappa_0 \beta_{en} \left\{ \frac{\alpha_{en} + \frac{C_A^{nC_{iA}} \left(1 - \frac{C_R^{nC_{iR}}}{k_{C_{iR}}^{nC_{iR}} + C_{iR}^{nC_{iR}}} \right)^{nC_{iA}}}{k_{C_{iA}}^{nC_{iA}} + C_{iA}^{nC_{iA}} \left(1 - \frac{C_R^{nC_{iR}}}{k_{C_{iR}}^{nC_{iR}} + C_{iR}^{nC_{iR}}} \right)^{nC_{iA}}} + \kappa_{En} \frac{En^{n_{En}}}{k_{DLEn}^{n_{En}} + En^{n_{En}}} - en}{\left(1 - \frac{En^{n_{En}}}{k_{DLEn}^{n_{En}} + En^{n_{En}}} \right)^{nC_{iA}}} \right\} \quad (8)$$

$$\frac{\partial En}{\partial t} = \theta_{en} en - \beta_{En} En \quad (9)$$

$$\frac{\partial eya}{\partial t} = \kappa_0 \beta_{eya} \left\{ \frac{\alpha_{Toy} C_{iA}^{nC_{iA}} \left(1 - \frac{Hth^{n_{Hth}}}{k_{Hth-eya}^{n_{Hth}} + Hth^{n_{Hth}}} \right)^{nC_{iA}}}{k_{C_{iA}eya}^{nC_{iA}} + C_{iA}^{nC_{iA}}} + \frac{\alpha_{eya} \left(1 - \frac{Hth^{n_{Hth}}}{k_{Hth-eya}^{n_{Hth}} + Hth^{n_{Hth}}} \right)^{nC_{iA}}}{k_{C_{iA}eya}^{nC_{iA}} + C_{iA}^{nC_{iA}}} + \frac{Eya^{n_{Eya}}}{k_{Eya}^{n_{Eya}} + Eya^{n_{Eya}}} - eya \right\} \quad (10)$$

$$\frac{\partial Eya}{\partial t} = \theta_{eya}eya - \beta_{Eya}Eya \quad (11)$$

$$\frac{\partial hth}{\partial t} = \kappa_0 \beta_{hth} \left\{ \frac{\alpha_{hth} + \alpha_{wg} \left(1 - \frac{Eya^{n_{Eya}}}{k_{Eya-hth}^{n_{Eya}} + Eya^{n_{Eya}}} \right)^{n_{wg}}}{k_{wg}^{n_{wg}} + \left(1 - \frac{Eya^{n_{Eya}}}{k_{Eya-hth}^{n_{Eya}} + Eya^{n_{Eya}}} \right)^{n_{wg}}} - hth \right\} \quad (12)$$

$$\frac{\partial Hth}{\partial t} = \theta_{hth}hth - \beta_{Hth}Hth \quad (13)$$

$$\delta(x) = \begin{cases} 1 & \text{if } x \in \text{hh-expressing cells} \\ 0 & \text{if } x \notin \text{hh-expressing cells} \end{cases} \quad (14)$$

RESULTS

Hh signaling and eyes absent expression are dynamic during ocellar patterning

In order to understand how the ocellar pattern (Fig. 1C) was generated, we analyzed the expression of *ptc* (a Hh signaling readout) and *eyes absent* (*eya*) (a Hh target) in the prospective ocellar region throughout L3. To monitor Ptc expression, we used a GFP:Ptc protein trap line. In early L3 discs, we detected a single domain of GFP:Ptc expression and uniformly low levels of Eya (Fig. 1D). By mid-L3, levels of Eya rise within the GFP:Ptc-expressing region, also as a single domain (Fig. 1E). From mid to late-L3, the final pattern arises through the repression of Ptc/Eya expression in the prospective interocellar cuticle (Fig. 1F). This pattern suggests the existence of a repressor capable of attenuating the *hh* pathway in the middle of the ocellar field [see also Brockmann et al. (Brockmann et al., 2011)] and whose expression and/or activity should build up during L3.

engrailed is activated by Hh and attenuates its signaling pathway to establish the ocellar pattern

engrailed (*en*) is a candidate *hh* repressor. It encodes a homeodomain transcription factor with an additional transcriptional repressor domain (Jaynes and O'Farrell, 1991). *En* is known to repress transcription of two major *hh* signaling components, *ptc* and *ci*, in embryos and wing imaginal discs (Eaton and Kornberg, 1990; Hidalgo and Ingham, 1990; Sanicola et al., 1995; Schwartz et al., 1995; Domínguez et al., 1996; Biehs et al., 2010). In the wing, *hh* expression in its posterior compartment depends on *en*. However, *hh* signaling from the posterior compartment induces *en* expression in anterior cells at a short range. Therefore, *en* is a low sensitivity *hh* target in the anterior wing (Guillén et al., 1995; Ohlmeyer and Kalderon, 1998; Méthot and Basler, 1999). In the ocellar region, *hh* expression precedes that of *en*, which is expressed in a *hh*-like pattern in late L3 (Royet and Finkelstein, 1996). These results suggest that *en* could be a *hh* target in the ocellar region. To test this point, we first checked the relative expression of *hh*, using the *hh-Z* strain as a *hh* transcriptional reporter, and of *en*. Their domains almost completely overlapped, with some *En*-only cells adjacent to the *hh-Z* domain (Fig. 2A). Second, when we knocked down the *hh* signaling pathway in *oc2 > GFP-PtcAloop2* discs, *en* expression was lost. The expression of *so*, which follows that of *eya*, was also lost from the ocellar region, confirming the effectiveness of the knock-down (Fig. 2B). This result indicated that *en* is a *hh* pathway target

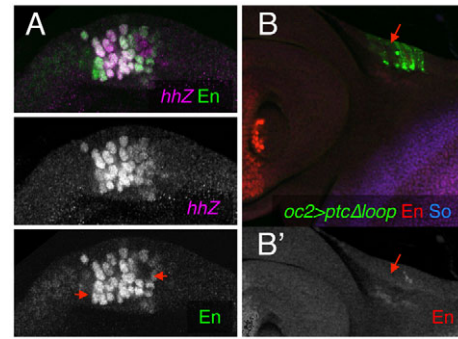


Fig. 2. *en* is a *hh*-signaling target. (A-B') Ocellar fields of late-L3 larvae. (A) *hh-Z* larva stained for β -galactosidase ('*hh-Z*') and anti-*En*. Individual channels are shown. The red arrows indicate nuclei expressing *En*, but not β -galactosidase. (B, B') *oc2>ptcAloop2-GFP* larva, stained for *En* and *So*. The expression of *ptcAloop2* is detected in the ocellar field as the GFP-positive patch (arrows). In this region, the *en* expression is almost totally absent. The *En* channel is shown separately (B'). In this genotype, *So* expression is also lost, indicating that the *hh*-signaling knock down induced by overexpression of *ptcAloop2* is effective.

in the ocellar region. To test for *en* function, we carried out three experiments. First, we verified the status of the *hh* signaling pathway in the *en*-expressing cells by examining *ci* expression. In the *en* domain, *ci* is repressed (Fig. 3A), a fact that is consistent with the repressor role of *en* in other developmental contexts. Second, to test directly this repressing role, we induced marked clones of cells homozygous for the *Df(2R)enE*. This deficiency removes both *en* and its paralog *invected* (*inv*), thus avoiding potential functional redundancy between both genes. In *Df(2R)enE* clones spanning the ocellar field the expression of Ptc and Ci is now continuous, lacking the characteristic gap in the prospective interocellar region (Fig. 3B). In adult mosaics, the anterior and posterior ocelli are often fused (Fig. 3C). The fact that the area of the fused ocelli is larger than the sum of the wild-type anterior and posterior ones suggests that the increase in ocellar surface is at the expense of interocellar cuticle. And third, we checked the effects of *en* overexpression on the *hh* target *eya*. In GFP-marked *en*-expressing clones, *eya* is repressed in a cell-autonomous manner (Fig. 3D). This *eya* loss could be explained either by *en* directly repressing *eya* or, indirectly, by *en* blocking the *hh* pathway. To distinguish between these two possibilities, we overexpressed *ci* throughout the ocellar field in *oc2>ci* larvae, therefore making *ci* transcription insensitive to *en* regulation. In these larvae, the expression of both *eya* and *en* is detected in most of the ocellar field (Fig. 3E,F). Therefore, Ci can activate *eya* even in the presence of *en*. In *oc2>ci* adults, the resulting ocellar complex is composed of a large, single ocellus, without interocellar cuticle (Fig. 3G). This indicates that *eya* is functionally epistatic over *en*, and suggests that the primary role of *en* is as a *hh* pathway regulator. In all, these results indicate that high concentrations of Hh result in high *en* expression, which in turn attenuates *hh* signaling in the middle of the ocellar field. As a consequence, RD expression and ocellar specification can only occur in regions that flank the *en* domain, which becomes the interocellar domain.

Delta:Notch signaling is required for *en* maintenance and interocellar region specification

en lays both downstream and upstream of the Hh signaling pathway, being activated by Hh and also repressing the pathway

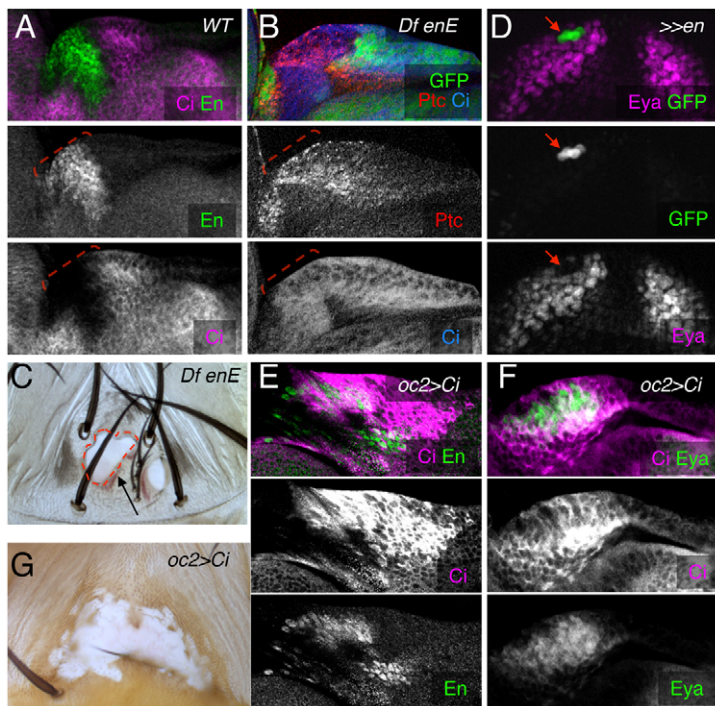


Fig. 3. *en* is a repressor of the *hh* pathway that is required for the interocellar region. (A,B,D-F) Ocellar fields of late-L3 larvae and (C,G) adult ocellar regions. (A) Wild-type ocellar field stained for En and Ci. The expression patterns of En and Ci are mutually exclusive. (B) A *DfenE* clone spanning the ocellar region. Within the mutant tissue (marked by the absence of GFP), Ptc and Ci are now expressed. The broken lines in A,B mark the approximate span of the En domain in a wild-type disc. (C) Ocellar region of an adult containing unmarked *DfenE* clones. A single ocellus extends over the whole left region (arrow). (D) Small *en*-expressing clone (>>*en*), marked with GFP, represses Eya cell-autonomously (arrows). (E,F) Ocellar fields from *oc2>ci* larvae express high levels of Ci (magenta). Both En (E) and Eya (F) are expressed in a single domain. In all immunofluorescence images, merged and separate channels are shown. (G) Ocellar region of a *oc2>ci* adult showing the enlargement of the ocelli and absence of interocellar cuticle. The fact that in this genotype both *en* and RD genes, such as *eya*, are expressed indicates that RD genes are functionally epistatic over *en*.

components *ci* and *ptc*. Therefore, these genetic relationships should lead to an unstable *en* expression (indeed, this conjecture was confirmed by our mathematical modeling, see below). Therefore, after its induction by *hh* signaling, an additional mechanism was required to stably maintain high levels of *en* expression in a *hh*-independent manner. It had been reported that in individuals mutant for a *Notch* temperature-sensitive (*N^{ts}*) allele, raised at the restrictive temperature during late larval life, the ocelli fuse (Amin, 2004), generating a ‘cyclopic’ ocellus similar to that observed in *Df(2R)enE* mosaics. To confirm the involvement of *Notch* signaling in ocellar development, we genetically manipulated several *Notch* pathway components. Ocellar-specific knock-downs of the nuclear transducer *Su(H)* [*Su(H)KD*] and the *Dl* ligand (*Dl KD*), or the overexpression of a dominant-negative

form of *mastermind* (*mamDN*), a *Notch* co-activator, resulted in expanded or fused ocelli (Fig. 4A; and not shown). Interestingly, similar knock down of the other *Notch* ligand, *Ser*, does not affect ocellar complex development (not shown). The similarity between the *Notch* pathway mutant phenotypes and the loss of *en* pointed to *Notch* signaling being required for *en* expression. Indeed, in *Su(H)KD* discs, the *en* domain is reduced in size and expression intensity and, concomitantly, the two RD domains extend, contacting each other (Fig. 4B,C).

In principle, the input of *Dl/Notch* in the network could be upstream of *hh* (maintaining its expression or signaling) or parallel to *hh*. However, the incomplete activation of *en* should persist in the former scenario. When we checked the signaling status of the *hh* pathway in *Su(H)KD* discs by analyzing *ptc* expression, we

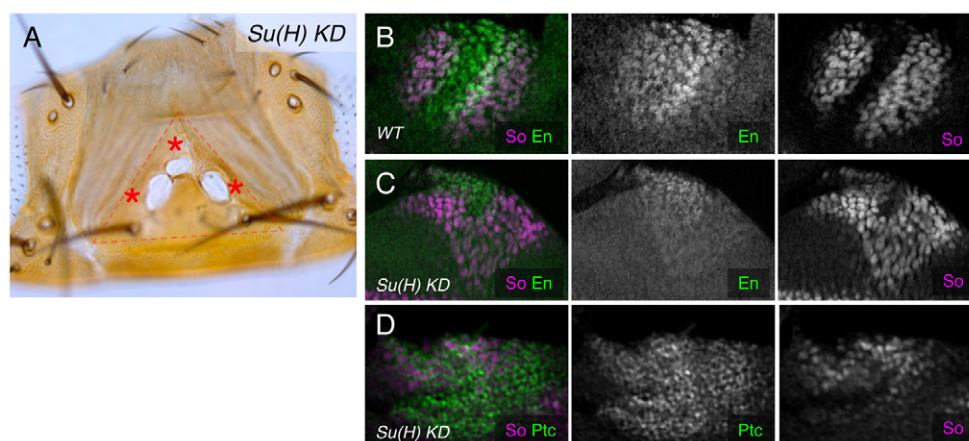


Fig. 4. *Notch* signaling is required for *en* expression and the specification of the interocellar region. (A) Adult dorsal head and (B-D) late-L3 ocellar fields. (A) A *oc2>Su(H) RNAi* [*Su(H)KD*] individual, showing enlarged ocelli (asterisks) at the expense of the interocellar region. No interocellar bristles remain. The ocellar complex region is marked by the triangle. (B) Wild-type expression of *en* and *so*. (C) In *Su(H)KD* discs, the *en* expression domain is weaker and smaller, whereas the *so* domains extend and fuse into a single domain. (D) In this genotype, the *hh* signaling pathway is not compromised, as strong Ptc signal is detected throughout the prospective ocellar field.

detected an unsplit domain of strong Ptc signal, indicative of sustained *hh* production and signaling when the activity of the *Notch* pathway is reduced (Fig. 4D). In addition, the fact that knocking down the *Notch* pathway still allowed specification of ocelli, which is a *hh*-controlled fate, agrees with *DI/Notch* acting parallel to, or downstream of, *hh*.

To determine the developmental window in which *Notch* signaling was required for the maintenance of *en*, we performed the following experiment. *DI* expression was knocked down at different times during third instar, taking advantage of the temperature sensitivity of the GAL4/UAS system (supplementary material Fig. S1; see also Materials and methods), and the size of the interocular cuticle in adults was analyzed, the fate of which depends on stable and high levels of *en* expression. Interocular cuticle surface was estimated by the number of interocular bristles formed (from 0 in its absence, to 6-8 in the wild type). Disconnecting *DI/Notch* signaling using a *UAS-DI-RNAi* (*oc2>DI-RNAi* or '*DI KD*') prior to 80 hours post fertilization (hpf) results in almost total absence of interocular cuticle. *DI KD* during the 80-85 hpf interval results in intermediate phenotypes with incomplete and variable interocular regions (supplementary material Fig. S1). Interestingly, this developmental window coincides with the establishment of a strong domain of *en* expression and the split of the *eya/so* domain in the disc (not shown). Knocking down *DI* after 85 hpf no longer precludes the generation of the interocular cuticle. This result shows that *Notch* signaling activity is required to establish the interocular fate during a short developmental interval (coinciding with upregulation of *en* in the ocellar field), after which, it remains stable. As the interocular fate depends on *en*, we interpret this result as *en* expression becoming fixed by *Notch* during the 80-85 hour interval.

A mathematical model for the Hh-driven ocellar patterning

In order to test whether our genetic reasoning was capable of generating the ocellar pattern, we developed a mathematical model incorporating all known genetic interactions (Fig. 5A). Several simplifications were made. First, the two-dimensional ocellar region is modeled as one dimensional (i.e. Fig. 5B, as a row of 31 cells). Second, the *hh* transcription domain (the central five cells) is set as a de facto in our model. Third, our model assumes that there is no proliferation during the developmental interval considered (see supplementary material Appendix S1). Hh production and diffusion have been modeled as in Eqn 1 (see Materials and methods), similar to the formalism used by Nahmad and Stathopoulos to model Hh gradient formation in the wing primordium, considering a diffusion coefficient of $D=0.5\mu\text{m}^2/\text{s}$ (Nahmad and Stathopoulos, 2009). Downstream of the Hh gradient, transcription and translation of all genes have been modeled using ordinary differential equations (ODEs), essentially following the modeling of the *Drosophila* embryonic segment polarity network by von Dassow and colleagues (von Dassow et al., 2000). Gene transcription may generally be affected by basal (b) and regulated transcription (T), and autoregulation (a), plus a decay term (Fig. 5C). Autoregulation is relevant only for *en* and *eya*. Transcriptional regulation terms have been modeled as sigmoids, allowing for potential cooperativity in transcriptional activation and repression. The general form of the transcription and translation equations, as well as the full set of equations are described in Materials and methods. In what follows, we explain how the new regulatory steps have been modeled. Further details on the specific biology underlying other equations (Eqns 2-7) are

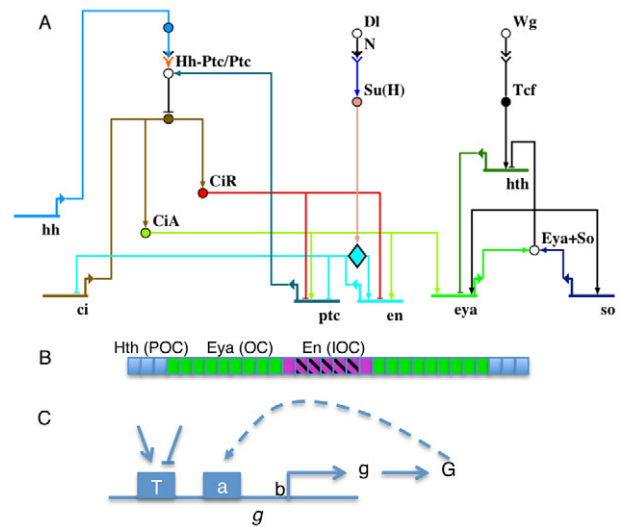


Fig. 5. Regulatory network and one-dimensional model.

(A) Biotapestry 'view from the genome' of the gene network. (B) One-dimensional lattice of 31 cells. *hh* is transcribed in the middle five cells (stripes). The target patterns for *Eya* (green), *En* (purple) and *Hth* (blue) are represented. These patterns correspond to the prospective ocellar (OC), interocular (IOC) and periocellar (POC) regions. (C) Generic gene (*g*) model. Transcript (*g*) and protein product (*G*) are indicated. The rate of transcription is dictated by basal transcription rate ('b'), regulated transcription, both positive and negative ('T'), and autoregulation ('a'). Decay rates applying to *g* and *G* and have not been represented.

described in supplementary material Appendix S1. We have shown that *DI/Notch* signaling is required for maintaining high *En* levels in the interocular region. We have modeled *en* maintenance as an autoregulation (Eqn 8), as *en* has been shown to autoregulate during embryo segmentation (Heemskerk et al., 1991). The contribution of *DI/Notch* signaling would be to facilitate the autoregulation of *en* by lowering *k* in the autoregulatory term (which indicates the *En* concentration for which half autoregulatory activation is reached). Because of this, it has been named k_{DIEn} . This implementation is the simplest form of representing the role of *DI/Notch* in allowing *en* autoregulation we could think of. It considers a constant and uniform *DI/Notch* input and that the *hh* and *Notch* pathway act independently of one another. The *en* autoregulation adds on top of a positive Hh signaling input on *en* transcription (Eqn 8). The expression of *eya* has been shown to depend only on *CiA* (Blanco et al., 2009), so no *CiR* input on *eya* regulation has been included. In addition, the *eya-so* positive-feedback loop (Pauli et al., 2005; Brockmann et al., 2011) has been collapsed into a direct *eya* autoregulation for simplicity (Eqn 10). In addition, previous results had suggested a mutual repression between *hth* and *eya* (Brockmann et al., 2011), which is probably direct (supplementary material Fig. S2). Therefore, *hth* has been modeled as a repressor input on *eya* (Eqn 10). In addition, *hth* transcription is modeled as being positively regulated by a constant term (α_{wg}) (Eqn 12), which represents the likely action of *Wnt1/wingless* (*wg*) (Azpiazu and Morata, 2000; Casares and Mann, 2000; Pichaud and Casares, 2000).

The working model has 61 free parameters. For a few, prior biological knowledge is helpful in defining at least some ranges. For example, the basal transcription rates of *ptc* and *ci* are positive, as these genes are widely transcribed. In order to generate a working set of parameter values that result in the target 'wild-type'

pattern (Fig. 5B, seven intercellular and two patches of nine ocellar cells in a 31 row), we first built a one-cell model in which to carry out the first parameter exploration. Then, this parameter set was used as a starting point to manually fine-tune the parameter values on the full model to reach a control pattern (see Materials and methods for further details). With this set of parameter values (supplementary material Table S1), the model accurately recapitulates the target pattern, including the dynamics of *Eya*, *Ptc*, *CiA*, *En* and *Hth* expression (Fig. 6; supplementary material Fig. S3). Modeling indicates that before reaching a steady state, the *Hh* gradient undergoes a transient expansion or ‘overshoot’ (Fig. 6A,B). This early dynamics depends on the non-linear *Ptc*-mediated feedback (Casali and Struhl, 2004; Nahmad and Stathopoulos, 2009). The model also predicts observed mutant behaviors, including the expansion of the ocellar tissue at the expense of intercellular cuticle in *Dl* and *en* loss-of-function mutants, or the effects of *hth* on ocellar size (supplementary material Fig. S4). Another computational experiment, the overexpression of *Dl*, predicted the expansion of the intercellular region at the expense of the ocelli. When this prediction was tested experimentally, by overexpressing *Dl* in the developing ocellar region (*oc2>Dl*), the intercellular region enlarged and the anterior ocellus disappeared (supplementary material Fig. S4).

The model GRN is robust against variations in initial conditions and noise

An important test for any systems behavior is the stability of its solution and whether this solution is unique or not. To test this point, the initial condition of every system variable was randomized (up to a 10-fold change) in each individual cell (supplementary material Table S2). The solution obtained for the system is stable, as the resulting patterns are the same as the wild type (supplementary material Fig. S5A). Only when the initial condition for *En* exceeds the concentration determined by the parameter k_{DIEn} , which is responsible for *En* autoregulation ($k_{DIEn} > 0.2$), is *en* expression fixed throughout, which precludes the

establishment of the *eya* pattern, as expected (supplementary material Fig. 5B,C). In fact, *En* expression is not detected in the ocellar region until mid-L3, after *Eya* expression has increased uniformly in the ocellar region (not shown).

Next, and to test whether the network topology is robust to fluctuations, we perturbed all parameters related with production and degradation rates ($\alpha_X, \theta_X, \beta_X$) with a uniform random signal (white noise). The noise amplitude was 20% for each corresponding rate (Fig. 7A). This fluctuation alters the evolution of the network elements as shown in the *Eya* time series of Fig. 7B. Under these conditions, the system reproduces the ocellar pattern with a slight deviation (widening) of the intercellular region. This experiment shows that indeed the network model is robust. To further test the robustness of the biological system, we subjected several *Drosophila* strains to temperature fluctuations during early L3, as a means to increase the noise in the system (Li et al., 2009). We included two reference strains as controls (the wild-type strain Oregon-R and w^{1118}) and stocks in which the gene dose of *smo*, *ptc*, *ci* and *Notch* is halved (see Materials and methods), and measured the longer axes of the anterior and posterior ocelli and the intercellular distance. These different genotypes can be thought of as representing the same gene network in which the parameter values may have different, genotype-specific, values. First, we found that different strains showed differences in ocellar and intercellular sizes, indicating that the genotype has a significant influence in the precise size and proportions within the ocellar complex (supplementary material Fig. S6). Second, and directly related to the aim of the experiment, we found that for some genotypes, the temperature fluctuation regime results in size deviations from the control. However, these deviations are smaller than the differences between genotypes. For example, while the difference in ocellar size between w^{1118} and *Notch*^{-/-} (at 25°C) is about 12%, the temperature fluctuations alter ocellar size in *Notch*^{-/-} by only 5%. Furthermore, the external noise introduced did not result in a significantly ‘noisier’ phenotype, measured as the coefficient of variation of ocellar and intercellular sizes

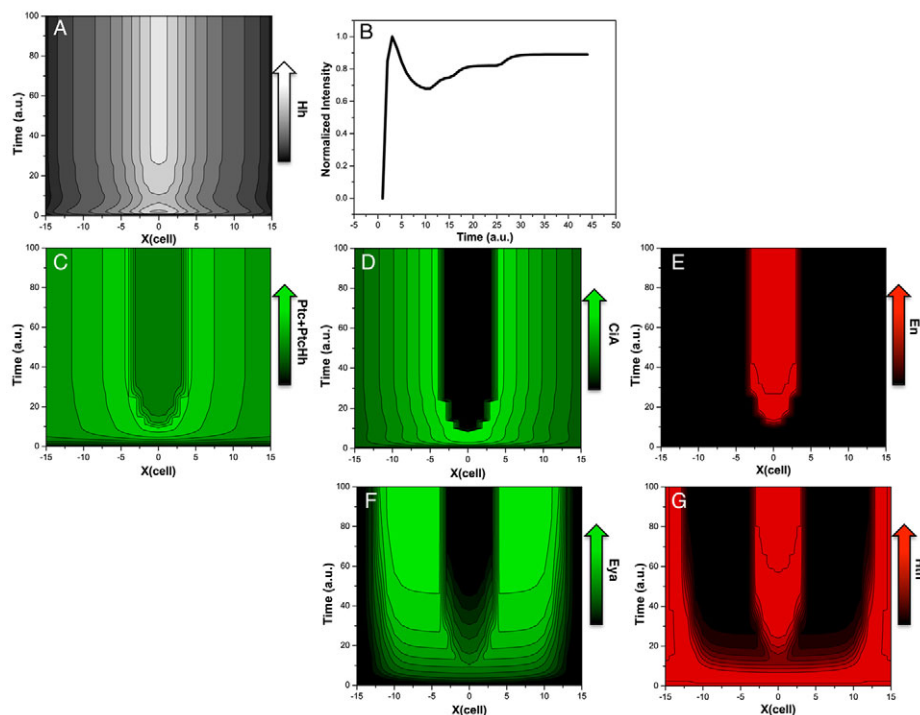


Fig. 6. Spatiotemporal dynamics of the Hh gradient and observed model variables. (A) Surface contour plot showing the Hh gradient dynamics. (B) Temporal variation of Hh concentration (normalized intensity) in cell 5. The magnitude of the Hh gradient varies with time, with an early ‘overshoot’, followed by a retraction to then reaching steady state. (C–G) Surface contour plots for the wild-type set of parameters depicting the dynamics of the variables that have been experimentally analyzed: total Ptc (*Ptc*+*Ptc*:Hh, C), *CiA* (D), *En* (E), *Eya* (F) and *Hth* (G). With this parameter set, the model correctly predicts qualitatively the biological pattern. (a.u.: arbitrary units). Cell number is represented on the x axis.

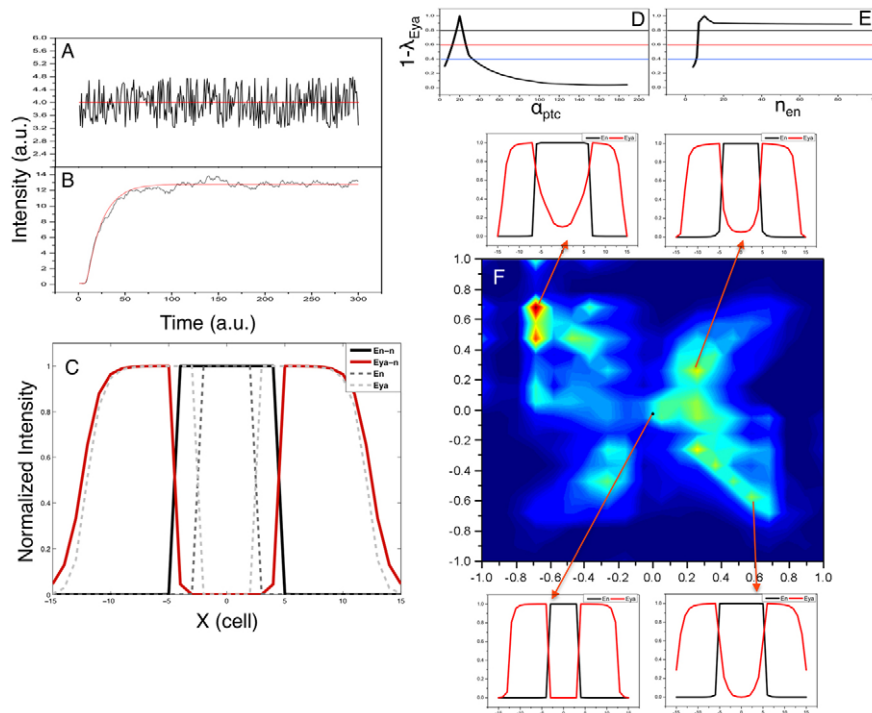


Fig. 7. Analysis of the robustness of the model against noise and parameter variations. (A) Application of a white noise distribution of 20% amplitude to θ_{en} as an example of noise implementation. (B) Eya time series with- and without-noise rates, shown in black and red. (C) Eya (red) and En (black) patterns when applying noise (continuous) or without noise (discontinuous). Rates with noise result in slightly broader intercellular region. (D,E) Examples of complementary distance when varying each parameter at a time over a range of two orders of magnitude. (D) α_{ptc} presents narrow ranges for ‘good’, ‘medium’ and ‘bad’ patterns [thresholds black (>0.8), red (0.6-0.8) and blue (0.4-0.6), respectively], while (E) η_{en} remains in the ‘good’ range in most of the studied range. (F) Density plot of 10,000 points in the 13-dimensional space corresponding to the distances of the 13 variable patterns to the wild type (black dot, situated at point 0,0). Some Eya and En patterns are also shown corresponding to the wild-type condition (bottom-left diagram) and three additional cases extracted from dense clusters located at different distances from the control.

(supplementary material Fig. S6). Therefore, the ocellar complex is robust against noise, as the model predicts. In addition, different genotypes, equivalent to the same gene network with a (presumably slightly) different set of parameter values, give rise to ocellar patterns that are also quantitatively different, even if these differences are small. The next section explores the properties of the model across the parameter space.

Exploration of parameter space suggests that the network imposes constraints on phenotypic variation

Next, we carried a parameter sensitivity assay. First, and starting with our working parameter set, we varied one parameter at a time in a two orders of magnitude range around its wild-type value, and measured the departure this variation caused from the wild-type pattern. As a metric for this deviation, we calculated a goodness score as a distance (λ) between the wild-type Eya pattern and that obtained from the varied parameter run, both normalized (see supplementary material Appendix S1). We established three thresholds for the complementarity of this distance ($1-\lambda$): $1-\lambda \geq 0.8$ (‘good’), $0.8 > 1-\lambda \geq 0.6$ (‘medium’) and $0.6 > 1-\lambda \geq 0.4$ (‘bad’), with $1-\lambda \geq 0.8$ being the most accurate fits (Fig. 7D,E; supplementary material Table S1). Twenty-eight out of 61 parameters gave goodness values above 0.8 over several orders of magnitude and were classified as ‘insensitive’ (i.e. large variations in their value did not result in major deviations from the target pattern) (Fig. 7E; supplementary material Fig. S9.1-9.4; supplementary material Table S1). The remaining ones (33) were sensitive (Fig. 7D), although the range of values for each specific parameter that resulted in a score of at least 0.8 varied among them (see supplementary material Table S1). The most sensitive parameter is the basal transcription rate constant α_{en} , which is also the parameter that does not allow variation in the noise experiments. This suggests that *en* expression has to be kept strictly off in the absence of patterned Hh signal. Not surprisingly, other sensitive parameters are those related to *ptc*

and *ci* expression, which affect the major feedbacks in the network (supplementary material Table S1).

Second, we carried out an analysis in which all 33 sensitive parameters were simultaneously randomized at each run inside one of the goodness intervals (the remaining parameters were left fixed at their wild-type values). A total of 10,000 runs were obtained, distributed among ‘good’ (6000), ‘medium’ (3000) and ‘bad’ (1000) randomized parameter values. For all 10,000 parameter sets, the distance for all the patterns of the system (one per variable) to the wild type was calculated. In this way, each parameter set defines a point in a 13-dimensional space, each dimension being one of the model variables (see supplementary material Appendix S1). For visualization, this information was reduced to three dimensions, two of them being the projections of the distance distributions two by two, and another representing the density of multidimensional points in such projections. The resulting 2D histogram (Fig. 7F; supplementary material Fig. S7) plots the density of patterns from the 10,000 randomized runs distributed relative to their distance from the wild type (point 0,0) (see supplementary material Appendix S1 for details). Therefore, it represents a map of the phenotypic space generated by the GRN (gene regulatory network) using randomized sets of parameters. Several conclusions can be derived from this analysis. First, the distribution of solutions (patterns) was not evenly dispersed. Instead, the solutions tended to concentrate in clusters or ‘islands’. Second, the wild-type pattern was placed inside a big and dense cluster, so this solution is highly probable, which indicates that the pattern is stable. Finally, when we analyzed the patterns of Eya and En (the two major readouts of the GRN) located in dense islands far apart from the wild type, we found that those patterns were still qualitatively similar to the wild type [Fig. 7F; see, for example, the high stability island around $(-0.7, 0.7)$ in supplementary material Fig. S7B]. This is interesting, because in this experiment we used parameter values coming not only from the ‘good’ interval, but also from ‘medium’ and ‘bad’ ones, as derived from our previous single parameter analysis. In summary, these analyses indicate that the

GRN is robust, because wide and random parameter variation results in specific phenotypic clusters, all of them similar to the wild type.

DISCUSSION

Many gene networks are described as static regulatory (activating and inhibitory) relationships between network components (genes and their products), disregarding essential dynamic and spatial aspects. In such descriptions, all genetic interactions are given as though happening at once and without spatial context. Mathematical modeling allows us to test the logic consistency of such networks, and whether or not they are capable of explaining the spatial and temporal dynamics of the biological system.

Using an integration of experimentation and mathematical network modeling, our results help to explain how several alternative fates are controlled by the Hh morphogen (Fig. 8). Previous descriptions of the genetic interactions involved in the specification and patterning of the ocellar complex structures did not offer satisfactory explanations for this fate choice decision.

A first important point is the addition to the GRN of *en* as a *hh* target with self-maintaining capability. The transduction of the Hh gradient generates an initial asymmetry, with only the cells receiving the highest Hh concentrations being able to maintain *en* expression. This in turn sets in motion the dynamics of the GRN. The evolution of some key system components is shown in Fig. 8.

A second important point is the action of *en* as a Hh-pathway repressor. The fact that *en* expression is sustained just in cells receiving the highest Hh concentrations (the Hh-producing cells and their adjacent neighbors) makes these cells read the Hh signal only transiently, as the signaling pathway is blocked as *en* expression builds up. This means that it would be impossible for

en to reach sufficient expression levels to shut off the pathway – and therefore, to inactivate *eya* – unless additional mechanisms were considered. In fact, the inactivation of *eya* is necessary for the specification of the interocular region: thus, uniform and high *ci* expression results in the co-expression of *eya* and *en* throughout the ocellar field. In this situation, *eya* is functionally epistatic over *en*, and the only tissue type specified is ocellus. Therefore, a stable interocular region can be established only if the initiation of *en* expression is followed by a *hh* signaling-independent phase. Such a transition from signal-induced expression to independent mode of maintenance has been reported for *en* during *Drosophila* embryonic segmentation (Heemskerk et al., 1991). In the ocellar field, we propose that this transition requires *Notch* signaling, specifically activated by its ligand *Dl* (but not by *Ser*). The molecular mechanisms of this *en* maintenance are not yet clear, but might involve PREs (polycomb response elements) in the *en* locus (Kwon et al., 2009).

Our model includes another repressor, *hth*, which enters the network as a direct repressor of RD. Its contribution seems limited to restricting the external extent of the *eya/so* expression domain. In *hthKD* animals, the ocelli are larger, but the interocular cuticle is still present. In our model, *en* repressive action suffices to turn off *hh* signaling pathway, thereby precluding RD activation. We have tested, through modeling, the possibility of *hth* being required for *en* activity, as it has been shown to be the case during embryonic segmentation (Kobayashi et al., 2003). In this case, though, making the repression function of *en* dependent on *hth* does not allow the network to reach any steady state in which the interocular domain is established – i.e. *en* does not reach the maintenance threshold. To verify this prediction, we checked *en* expression and the activity status of the *hh* pathway in *hthKD* discs. As predicted, *en* is expressed at normal levels in a domain where *ci* is off, as in wild type (supplementary material Fig. S8).

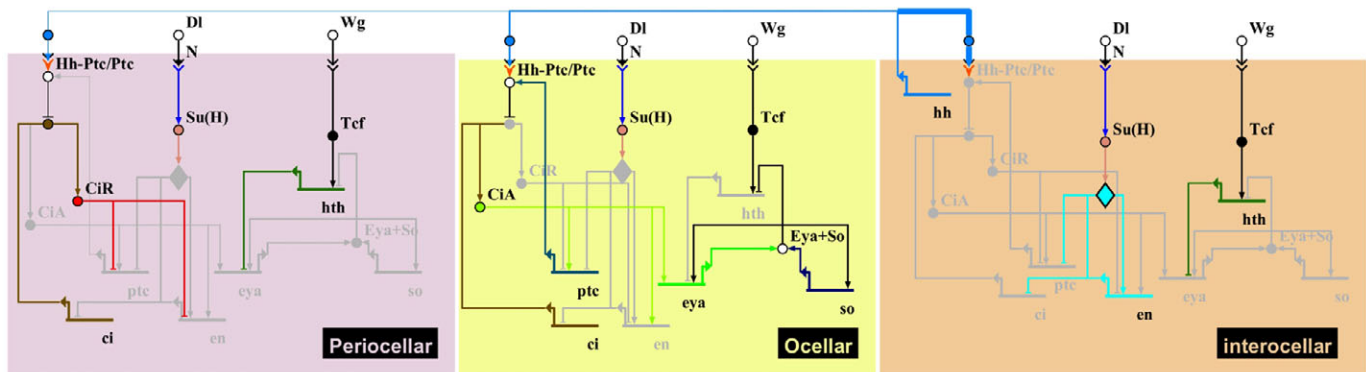


Fig. 8. Logic of the ocellar complex GRN. A Biotapestry representation of the ocellar complex (OC) GRN architecture. Genes are represented by horizontal lines topped by a bent arrow (the transcriptional start site, TSS). Positive and negative interactions (lines emerging from the TSS) are represented by arrows or capped lines, respectively. Protein-protein interactions are represented by circles. Different cell types are symbolized with colored boxes (named accordingly). Cell signaling is represented by lines reaching from inside one cell type to the outside (thickness indicates strength of the signaling); chevrons and circles are used to represent signal reception and transduction, respectively. White circles outside cell boxes represent signaling ligands. Genes and interactions are represented in color if active, in gray otherwise. Three cell types are specified according to the decreasing level of Hh signal they receive: inter-ocular, ocellar and periocular cells. Hh signal triggers both RD genes (*eya* and *so*) and *en* expression. In interocular cells, high Hh concentrations promote the expression of *en*, which in turn represses RD genes by shutting down *ptc* and *ci* expression, and therefore eliminating Hh signal reception. Inside ocellar cells, *en* expression does not occur because of weaker Hh signaling; this makes RD gene activation possible. Ocellar and interocular cells therefore achieve distinct gene expression patterns. In interocular cells, *en* expression is maintained by the *Dl/Notch* pathway (present throughout the entire OC). This particular interaction is represented with a diamond (within the *en* auto-activation line). RD genes expression domain is also defined through the contribution of *hth*; this gene is likely to be activated downstream of the *wg* pathway. In ocellar cells, Eya and So (acting as a complex) repress *hth*. Periocular cells lie at the periphery of Hh signaling and RD gene activation is prevented by Hth: this repression contributes to define the size of the ocelli. The periocular region gives rise to the front cuticle in the adult head.

Recently, a similar situation to the one we detailed here has been described during the dorsoventral patterning of the vertebrate neural tube by *Shh* (Ribes et al., 2010). The floor plate (FP), the ventral-most region of the neural tube, expresses *Shh* and requires maximal *Shh* concentrations for its specification (Chiang et al., 1996; Ericson et al., 1996). However, this requirement is transient and followed by an attenuation of the pathway. This attenuation is necessary for FP specification (Ribes et al., 2010). This process of FP specification is reminiscent of the specification of the interocellar cuticle in our system. This similarity raises the possibility that a negative-feedback loop in the *Shh* pathway, of the type we have described here, could be part of the neural tube GRN. However, after the initial asymmetry within the ocellar field has been established, an external input, the *Dl/Notch* signal, is needed to maintain it. In our model, there is no need for a localized *Notch* signal: uniform signaling suffices, provided that *en* expression reaches a specific concentration threshold. In fact, using an anti-*Dl* monoclonal antibody, we detect uniform levels of *Dl* expression in the ocellar field in mid-L3 (not shown), the developmental period when we start to see the distinct domains emerging. Interestingly, a recent report finds an association between mutations in *Dll1*, a vertebrate *Dl*-like ligand, and holoprosencephaly (Dupé et al., 2011). Holoprosencephaly, a developmental defect caused by abnormal specification of the ventral midline structures of the anterior neural tube, is frequently associated with malfunction of the *Shh* pathway. In fact, work in vertebrates indicates that *Notch* signaling is indeed required for FP fate acquisition parallel to *Shh* (le Roux et al., 2003; Peyrot et al., 2011). It is therefore tempting to speculate that the *Notch* pathway is required to fix the FP fate in the vertebrate neural tube by stabilizing gene expression during the phase of *Shh* signaling attenuation, as we propose here for *Notch* in the *Drosophila* ocellar GRN.

The model we have described explains how mutually exclusive gene expression domains are produced under the control of a Hh gradient by connecting a repressive gene circuitry. These expression domains underlie the morphology of the structures that will later form and cannot be explained unless the information of Hh gradient is integrated with the logic of the GRN. They can therefore be considered as the emerging properties of the system we have described.

The structure of this GRN confers robustness to the patterning mechanism, buffering variations in the initial conditions, as well as absorbing noise. Although the model predicts an early overshoot of the Hh gradient, this might not be crucial, as variations in the initial conditions converge to the same pattern.

Interestingly, random variation of parameter values results in the system deviating from the ‘wild-type’ pattern in a non-random manner, but instead falling into specific ‘islands’ of the phenotypic space. That is, variations in the control parameters of the GRN generate phenotypes that maintain certain rules of proportionality. Still these phenotypic ‘variants’ are robust against noise, as is the wild-type pattern (supplementary material Fig. S7). These mathematical properties of the ocellar network might ensure the phenotypic stability of the ocellar structures in wild flies exposed to varying environmental conditions during development, as well as constraining the phenotypic variability of the ocelli during evolution.

Acknowledgements

We thank I. Guerrero, I. Rebay and R. S. Mann for antibodies; P. Rojas, J. Blanco, C. M. Luque, the Bloomington, VDRC and Flytrap Stock Centers, and the Consolider ‘From Genes to Shape’ *Drosophila* Collection for fly strains; and O. Abreu for help with experiments.

Funding

This work was funded by the Spanish Ministry for Science and Innovation (MICINN/MINECO, co-funded by Feder program) [BFU2009-07044], by Proyecto de Excelencia CVI 2658 (Junta de Andalucía) to F.C., by Consolider ‘From Genes to Shape’ (in which F.C. is participant researcher; MICINN/MINECO), and by MICINN/MINECO [FIS2008-04120 to A.C. and M.C.L.].

Competing interests statement

The authors declare no competing financial interests.

Supplementary material

Supplementary material available online at <http://dev.biologists.org/lookup/suppl/doi:10.1242/dev.082172/-/DC1>

References

- Alexandre, C., Jacinto, A. and Ingham, P. W. (1996). Transcriptional activation of hedgehog target genes in *Drosophila* is mediated directly by the cubitus interruptus protein, a member of the GLI family of zinc finger DNA-binding proteins. *Genes Dev.* **10**, 2003-2013.
- Amin, A. (2004). Genetic cross-talk during head development in *Drosophila*. *J. Biomed. Biotechnol.* **2004**, 16-23.
- Aza-Blanc, P., Ramírez-Weber, F. A., Laget, M. P., Schwartz, C. and Kornberg, T. B. (1997). Proteolysis that is inhibited by hedgehog targets Cubitus interruptus protein to the nucleus and converts it to a repressor. *Cell* **89**, 1043-1053.
- Azpiazu, N. and Morata, G. (2000). Function and regulation of homothorax in the wing imaginal disc of *Drosophila*. *Development* **127**, 2685-2693.
- Balaskas, N., Ribeiro, A., Panovska, J., Dessaud, E., Sasai, N., Page, K. M., Briscoe, J. and Ribes, V. (2012). Gene regulatory logic for reading the Sonic Hedgehog signaling gradient in the vertebrate neural tube. *Cell* **148**, 273-284.
- Basler, K. and Struhl, G. (1994). Compartment boundaries and the control of *Drosophila* limb pattern by hedgehog protein. *Nature* **368**, 208-214.
- Bessa, J. and Casares, F. (2005). Restricted teashirt expression confers eye-specific responsiveness to Dpp and Wg signals during eye specification in *Drosophila*. *Development* **132**, 5011-5020.
- Biehls, B., Kechris, K., Liu, S. and Kornberg, T. B. (2010). Hedgehog targets in the *Drosophila* embryo and the mechanisms that generate tissue-specific outputs of Hedgehog signaling. *Development* **137**, 3887-3898.
- Blanco, J., Seimiya, M., Pauli, T., Reichert, H. and Gehring, W. J. (2009). Wingless and Hedgehog signaling pathways regulate orthodenticle and eyes absent during ocelli development in *Drosophila*. *Dev. Biol.* **329**, 104-115.
- Blanco, J., Pauli, T., Seimiya, M., Udolph, G. and Gehring, W. J. (2010). Genetic interactions of eyes absent, twin of eyeless and orthodenticle regulate sine oculis expression during ocellar development in *Drosophila*. *Dev. Biol.* **344**, 1088-1099.
- Bonini, N. M., Leiserson, W. M. and Benzer, S. (1993). The eyes absent gene: genetic control of cell survival and differentiation in the developing *Drosophila* eye. *Cell* **72**, 379-395.
- Bonini, N. M., Leiserson, W. M. and Benzer, S. (1998). Multiple roles of the eyes absent gene in *Drosophila*. *Dev. Biol.* **196**, 42-57.
- Briscoe, J., Chen, Y., Jessell, T. M. and Struhl, G. (2001). A hedgehog-insensitive form of patched provides evidence for direct long-range morphogen activity of sonic hedgehog in the neural tube. *Mol. Cell* **7**, 1279-1291.
- Brockmann, A., Domínguez-Cejudo, M. A., Amore, G. and Casares, F. (2011). Regulation of ocellar specification and size by twin of eyeless and homothorax. *Dev. Dyn.* **240**, 75-85.
- Buszczak, M., Paterno, S., Lighthouse, D., Bachman, J., Planck, J., Owen, S., Skora, A. D., Nystul, T. G., Ohlstein, B., Allen, A. et al. (2007). The carnegie protein trap library: a versatile tool for *Drosophila* developmental studies. *Genetics* **175**, 1505-1531.
- Casali, A. and Struhl, G. (2004). Reading the Hedgehog morphogen gradient by measuring the ratio of bound to unbound Patched protein. *Nature* **431**, 76-80.
- Casares, F. and Mann, R. S. (2000). A dual role for homothorax in inhibiting wing blade development and specifying proximal wing identities in *Drosophila*. *Development* **127**, 1499-1508.
- Chen, Y. and Struhl, G. (1996). Dual roles for patched in sequestering and transducing Hedgehog. *Cell* **87**, 553-563.
- Cheyette, B. N., Green, P. J., Martin, K., Garren, H., Hartenstein, V. and Zipursky, S. L. (1994). The *Drosophila* sine oculis locus encodes a homeodomain-containing protein required for the development of the entire visual system. *Neuron* **12**, 977-996.
- Chiang, C., Litingtung, Y., Lee, E., Young, K. E., Corden, J. L., Westphal, H. and Beachy, P. A. (1996). Cyclopia and defective axial patterning in mice lacking Sonic hedgehog gene function. *Nature* **383**, 407-413.
- Davidson, E. H. (2006) *The Regulatory Genome: Gene Regulatory Networks in Development and Evolution*. San Diego, CA: Academic Press.
- Dessaud, E., Yang, L. L., Hill, K., Cox, B., Ulloa, F., Ribeiro, A., Mynett, A., Novitsch, B. G. and Briscoe, J. (2007). Interpretation of the sonic hedgehog

- morphogen gradient by a temporal adaptation mechanism. *Nature* **450**, 717-720.
- Dessaud, E., McMahon, A. P. and Briscoe, J.** (2008). Pattern formation in the vertebrate neural tube: a sonic hedgehog morphogen-regulated transcriptional network. *Development* **135**, 2489-2503.
- Dessaud, E., Ribes, V., Balaskas, N., Yang, L. L., Pierani, A., Kicheva, A., Novitsch, B. G., Briscoe, J. and Sasai, N.** (2010). Dynamic assignment and maintenance of positional identity in the ventral neural tube by the morphogen sonic hedgehog. *PLoS Biol.* **8**, e1000382.
- Dominguez, M., Brunner, M., Hafen, E. and Basler, K.** (1996). Sending and receiving the hedgehog signal: control by the Drosophila Gli protein Cubitus interruptus. *Science* **272**, 1621-1625.
- Dupé, V., Rochard, L., Mercier, S., Le Pétilion, Y., Gicquel, I., Bendavid, C., Bourrouillou, G., Kini, U., Thauvin-Robinet, C., Bohan, T. P. et al.** (2011). NOTCH, a new signaling pathway implicated in holoprosencephaly. *Hum. Mol. Genet.* **20**, 1122-1131.
- Eaton, S. and Kornberg, T. B.** (1990). Repression of *ci-D* in posterior compartments of Drosophila by engrailed. *Genes Dev.* **4**, 1068-1077.
- Ericson, J., Morton, S., Kawakami, A., Roelink, H. and Jessell, T. M.** (1996). Two critical periods of Sonic Hedgehog signaling required for the specification of motor neuron identity. *Cell* **87**, 661-673.
- Finkelstein, R., Smouse, D., Capaci, T. M., Spradling, A. C. and Perrimon, N.** (1990). The orthodenticle gene encodes a novel homeo domain protein involved in the development of the Drosophila nervous system and ocellar visual structures. *Genes Dev.* **4**, 1516-1527.
- Freeman, M. and Gurdon, J. B.** (2002). Regulatory principles of developmental signaling. *Annu. Rev. Cell Dev. Biol.* **18**, 515-539.
- González, A., Chaouiya, C. and Thieffry, D.** (2008). Logical modelling of the role of the Hh pathway in the patterning of the Drosophila wing disc. *Bioinformatics* **24**, i234-i240.
- Guillé, I., Mullor, J. L., Capdevila, J., Sánchez-Herrero, E., Morata, G. and Guerrero, I.** (1995). The function of engrailed and the specification of Drosophila wing pattern. *Development* **121**, 3447-3456.
- Haynie, J. L. and Bryant, P. J.** (1986). Development of the eye-antenna imaginal disc and morphogenesis of the adult head in Drosophila melanogaster. *J. Exp. Zool.* **237**, 293-308.
- Heemskerck, J., DiNardo, S., Kostriken, R. and O'Farrell, P. H.** (1991). Multiple modes of engrailed regulation in the progression towards cell fate determination. *Nature* **352**, 404-410.
- Hidalgo, A. and Ingham, P.** (1990). Cell patterning in the Drosophila segment: spatial regulation of the segment polarity gene *patched*. *Development* **110**, 291-301.
- Ingham, P. W., Nakano, Y. and Seger, C.** (2011). Mechanisms and functions of Hedgehog signalling across the metazoa. *Nat. Rev. Genet.* **12**, 393-406.
- Irons, D. J., Wojcinski, A., Glise, B. and Monk, N. A.** (2010). Robustness of positional specification by the Hedgehog morphogen gradient. *Dev. Biol.* **342**, 180-193.
- Jaynes, J. B. and O'Farrell, P. H.** (1991). Active repression of transcription by the engrailed homeodomain protein. *EMBO J.* **10**, 1427-1433.
- Jiang, J. and Hui, C. C.** (2008). Hedgehog signaling in development and cancer. *Dev. Cell* **15**, 801-812.
- Kobayashi, M., Fujioka, M., Tolkunova, E. N., Deka, D., Abu-Shaar, M., Mann, R. S. and Jaynes, J. B.** (2003). Engrailed cooperates with extradenticle and homothorax to repress target genes in Drosophila. *Development* **130**, 741-751.
- Kumar, J. P. and Moses, K.** (2001). EGF receptor and Notch signaling act upstream of Eyeless/Pax6 to control eye specification. *Cell* **104**, 687-697.
- Kwon, D., Mucci, D., Langlais, K. K., Americo, J. L., DeVido, S. K., Cheng, Y. and Kassis, J. A.** (2009). Enhancer-promoter communication at the Drosophila engrailed locus. *Development* **136**, 3067-3075.
- le Roux, I., Lewis, J. and Ish-Horowitz, D.** (2003). Notch activity is required to maintain floorplate identity and to control neurogenesis in the chick hindbrain and spinal cord. *Int. J. Dev. Biol.* **47**, 263-272.
- Li, X., Cassidy, J. J., Reinke, C. A., Fischboeck, S. and Carthew, R. W.** (2009). A microRNA imparts robustness against environmental fluctuation during development. *Cell* **137**, 273-282.
- Marigo, V. and Tabin, C. J.** (1996). Regulation of *patched* by sonic hedgehog in the developing neural tube. *Proc. Natl. Acad. Sci. USA* **93**, 9346-9351.
- Méthot, N. and Basler, K.** (1999). Hedgehog controls limb development by regulating the activities of distinct transcriptional activator and repressor forms of Cubitus interruptus. *Cell* **96**, 819-831.
- Mutsuddi, M., Chaffee, B., Cassidy, J., Silver, S. J., Tootle, T. L. and Rebay, I.** (2005). Using Drosophila to decipher how mutations associated with human branchio-oto-renal syndrome and optical defects compromise the protein tyrosine phosphatase and transcriptional functions of eyes absent. *Genetics* **170**, 687-695.
- Nahmad, M. and Stathopoulos, A.** (2009). Dynamic interpretation of hedgehog signaling in the Drosophila wing disc. *PLoS Biol.* **7**, e1000202.
- Nakano, Y., Guerrero, I., Hidalgo, A., Taylor, A., Whittle, J. R. and Ingham, P. W.** (1989). A protein with several possible membrane-spanning domains encoded by the Drosophila segment polarity gene *patched*. *Nature* **341**, 508-513.
- Ohlmeyer, J. T. and Kalderon, D.** (1998). Hedgehog stimulates maturation of Cubitus interruptus into a labile transcriptional activator. *Nature* **396**, 749-753.
- Pauli, T., Seimiya, M., Blanco, J. and Gehring, W. J.** (2005). Identification of functional sine oculis motifs in the autoregulatory element of its own gene, in the eyeless enhancer and in the signalling gene hedgehog. *Development* **132**, 2771-2782.
- Peyrot, S. M., Wallingford, J. B. and Harland, R. M.** (2011). A revised model of Xenopus dorsal midline development: differential and separable requirements for Notch and Shh signaling. *Dev. Biol.* **352**, 254-266.
- Pichaud, F. and Casares, F.** (2000). homothorax and irouquois-C genes are required for the establishment of territories within the developing eye disc. *Mech. Dev.* **96**, 15-25.
- Probst, S., Kraemer, C., Demougin, P., Sheth, R., Martin, G. R., Shiratori, H., Hamada, H., Iber, D., Zeller, R. and Zuniga, A.** (2011). SHH propagates distal limb bud development by enhancing CYP26B1-mediated retinoic acid clearance via AER-FGF signalling. *Development* **138**, 1913-1923.
- Punzo, C., Seimiya, M., Flister, S., Gehring, W. J. and Plaza, S.** (2002). Differential interactions of eyeless and twin of eyeless with the sine oculis enhancer. *Development* **129**, 625-634.
- Ribes, V., Balaskas, N., Sasai, N., Cruz, C., Dessaud, E., Cayuso, J., Tozer, S., Yang, L. L., Novitsch, B., Marti, E. et al.** (2010). Distinct Sonic Hedgehog signaling dynamics specify floor plate and ventral neuronal progenitors in the vertebrate neural tube. *Genes Dev.* **24**, 1186-1200.
- Royet, J. and Finkelstein, R.** (1995). Pattern formation in Drosophila head development: the role of the orthodenticle homeobox gene. *Development* **121**, 3561-3572.
- Royet, J. and Finkelstein, R.** (1996). hedgehog, wingless and orthodenticle specify adult head development in Drosophila. *Development* **122**, 1849-1858.
- Royet, J. and Finkelstein, R.** (1997). Establishing primordia in the Drosophila eye-antennal imaginal disc: the roles of decapentaplegic, wingless and hedgehog. *Development* **124**, 4793-4800.
- Saha, K. and Schaffer, D. V.** (2006). Signal dynamics in Sonic hedgehog tissue patterning. *Development* **133**, 889-900.
- Sanicola, M., Sekelsky, J., Elson, S. and Gelbart, W. M.** (1995). Drawing a stripe in Drosophila imaginal disks: negative regulation of decapentaplegic and patched expression by engrailed. *Genetics* **139**, 745-756.
- Schwartz, C., Locke, J., Nishida, C. and Kornberg, T. B.** (1995). Analysis of cubitus interruptus regulation in Drosophila embryos and imaginal disks. *Development* **121**, 1625-1635.
- Serikaku, M. A. and O'Tousa, J. E.** (1994). Sine oculis is a homeobox gene required for Drosophila visual system development. *Genetics* **138**, 1137-1150.
- Tabata, T., Schwartz, C., Gustavson, E., Ali, Z. and Kornberg, T. B.** (1995). Creating a Drosophila wing de novo, the role of engrailed, and the compartment border hypothesis. *Development* **121**, 3359-3369.
- Varjosalo, M. and Taipale, J.** (2008). Hedgehog: functions and mechanisms. *Genes Dev.* **22**, 2454-2472.
- von Dassow, G., Meir, E., Munro, E. M. and Odell, G. M.** (2000). The segment polarity network is a robust developmental module. *Nature* **406**, 188-192.
- Wang, L. H., Huang, Y. T., Tsai, Y. C. and Sun, Y. H.** (2010). The role of eyg Pax gene in the development of the head vertex in Drosophila. *Dev. Biol.* **337**, 246-258.
- Wieschaus, E., Perrimon, N. and Finkelstein, R.** (1992). orthodenticle activity is required for the development of medial structures in the larval and adult epidermis of Drosophila. *Development* **115**, 801-811.
- Xu, T. and Rubin, G. M.** (1993). Analysis of genetic mosaics in developing and adult Drosophila tissues. *Development* **117**, 1223-1237.